Desalination and Water Treatment
www.deswater.com
doi: 10.1080/19443994.2014.960460

56 (2015) 2023–2036
November

Taylor & Francis
Taylor & Francis Group

CFD analysis of vapor flow and design improvement in MED evaporation chamber

M. Khamis Mansour[a,1,*], M.A. Qassem[a], Hassan Fath[b,2]

[a]*Faculty of Engineering, Mechanical Department, Alexandria University, Elhorreya Road P.O. 21544, Alexandria, Egypt, Tel. +20 3591 0052; Fax: +20 3597 1853; email: mdkhamis@gmail.com (M. Khamis Mansour)*
[b]*Department of Energy Resources and Environmental Engineering, Egypt-Japan University of Science & Technology—EJUST, P.O. Box 179, New Borg El-Arab City, Alexandria 21934, Egypt, Tel./Fax: +203 459 9520*

Received 10 March 2014; Accepted 24 August 2014

ABSTRACT

This paper presents the Computational Fluid Dynamics (CFD) analysis of the vapor flow inside the Evaporation Chamber (EC) of a two-effect Multi-Effect Distillation (MED) unit. The study is part of the EU–Egypt funded project Multipurpose Applications by Thermodynamics Solar. The numerical analysis investigates the effect of velocity variations on the EC's carryover factor and demister pressure drop for different separation baffle configurations. The trajectory of liquid droplets was calculated using Lagrange approach. The computational model was verified by comparing the predicated results (vapor pressure drop through the demister and separation efficiency) with those obtained from published data, with good agreement. At the design inlet vapor velocity of 3.3 m/s, a new baffle configuration is presented and is characterized by the best performance among the other configurations. This new baffle configuration shows a minimum carryover factor of 0.097 with a reasonable demister pressure drop less than 13.4% of the originally designed one. The study could be considered a benchmark and a helpful guideline for future designs of MED-EC.

Keywords: Desalination; MED; Demister; Separation efficiency; Droplets trajectory; Lagrange model; CFD

1. Introduction

The growth of desalination technology is steadily increasing with more interest in Multi-Effect Distillation (MED). MED systems are well known thermodynamically as the most efficient of all thermal distillation processes [1], but their widespread usage may be hindered by scaling problems when efforts are made to raise water production with higher top brine temperatures [2]. In MED, the specific energy consumption to produce one cubic meter of desalinated water is considerably less than that obtained from other thermal technologies such as Multi-Stage Flash (MSF) distillation. MED technology attracts many

*Corresponding author.
[1]Present address: Faculty of Engineering, Mechanical Department, Beirut Arab University, P.O. Box 115020 Riad El Solh, 11072809 Beirut, Lebanon.
[2]Faculty of Engineering, Mechanical Department, Alexandria University, Alexandria, Egypt.

studies, particularly those related to hybridize MED with other desalination systems, such as MED-RO and MED-MSF. Recently, different researches have been conducted to analyze new hybrid systems, theoretically and experimentally, [3–5] for MED-adsorption systems and [6–8] for MED connected to an absorption heat pump. Therefore, there is always a need to understand how the thermal and hydraulic performances of MED units can be improved, and thus, in turn, ultimately reduce the specific energy consumption and the specific cost of the product water.

The Multipurpose Applications by Thermodynamic Solar (MATS) project is an EU–Egypt jointly funded project (Fig. 1). The MATS project aims at promoting the exploitation of concentrated solar power through small- and middle-scale facilities, suitable to fulfill local requirements of power and water. A MED unit is placed at the end of the solar steam power cycle to use the low-grade exhausted steam coming from the turbine. As the result of water scarcity at the selected site (of new Borg Al-Arab, Alexandria, Egypt), an air-cooled condenser is used.

Fig. 2 shows the schematic diagram of MATS's MED-EC unit. The MED unit consists only of two effects. Heating steam is introduced into the tubes of the first effect while the vapor generated in the second effect flows into the unit condenser. Similar to conventional MED, heating steam condenses into distillate inside the tubes while the feed water warms up and partly evaporates by recovering the condensation heat. Due to evaporation, feed water slightly concentrates when flowing down the bundle and the brine is drained at the bottom of the second effect.

The separation baffle and the demister are considered the main components inside the MED-EC. They are responsible for achieving high-quality distillated water by retaining the salted liquid droplets to be entrained with the vapor flow to the next effect, as shown in Fig. 2. These moisture separation components should be featured by higher separation efficiency with lower pressure drop to render the best thermal and hydraulic performances to the unit. The higher the pressure drop, the higher the losses in the temperature driving force between the effects. Alternatively, the lower the separation efficiency, the higher the brine carryover that causes lower product water quality and possible scales in the condenser tubes, harming the unit's thermal performance. Wire mesh demister is the most widely used in MED and MSF plants as a result of its features of low pressure drop, high separation efficiency, and reasonable capital cost. In this study, the wire mesh demister was used as planned in the MATS project MED unit.

The literature review of the demister performance evaluation is classified into two categories. The first focuses on empirical or semi-empirical correlations obtained for the separation/removal efficiency and the pressure drop across the demister. The second one is related to numerical studies using CFD modeling to simulate the demister performance. El-Dessouky et al. [9] presented an empirical model for the pressure drop and the separation efficiency for the wire mesh demister pad. The correlation of the separation efficiency is a function of vapor velocity, wire diameter, droplet size, and packing density. As the wet pressure drop is affected by the packing density, wire diameter, and vapor velocity, Brunazzi and Paglianti [10] presented a semi-empirical model for the demister design, which is built on previous analysis presented by Langmuir and Blodgett [11], and Pich [12]. The authors evaluated the inertial capture efficiency for a single wire, expressed in terms of a dimensionless Stokes number. The analysis of the industrial wire mesh packing is presented by Carpenter and Othmer [13] as a function of the demister pad thickness, the demister specific area, the Stokes efficiency, and the number of mesh layers. A new model was presented by Brunazzi and Paglianti [14] for predicting the removal efficiency of complex wire mesh eliminators. This new model can be used for predicting the separation efficiency of multilayer pads and composite separators.

On the other hand, limited research is found in the literature on demister separation efficiency using CFD technique. CFD studies were presented on two types of demisters: waveplate (vane type) demisters and wire mesh demisters. Wang and Davies [15] used the commercial software Phoenics to carry out a comprehensive numerical investigation on the effect of inlet gas velocity, bend angle, and rear pockets on separation efficiency and pressure drop of the waveplate demister. They used the Eulerian–Lagrangian approach in order to track the liquid droplets. The droplets had uniform diameters of 10, 15, and 20 μm, respectively. A standard k–ε turbulence model was used to simulate the gaseous phase; turbulent dispersion effects on droplet trajectories were not taken into account. No comparison with experimental data was provided. Gillandt et al. [16] used the commercial software Fluent to simulate the flow in a zigzag classifier, comparing experimental and predicted data. The droplet size investigated ranged from 0.1 to 1 mm. The authors pointed out that the use of a low Re k–ε turbulence model gives better results than the standard version of the model. Wang and James [17] investigated the separation efficiency of two waveplate demisters by numerically simulating the flow field

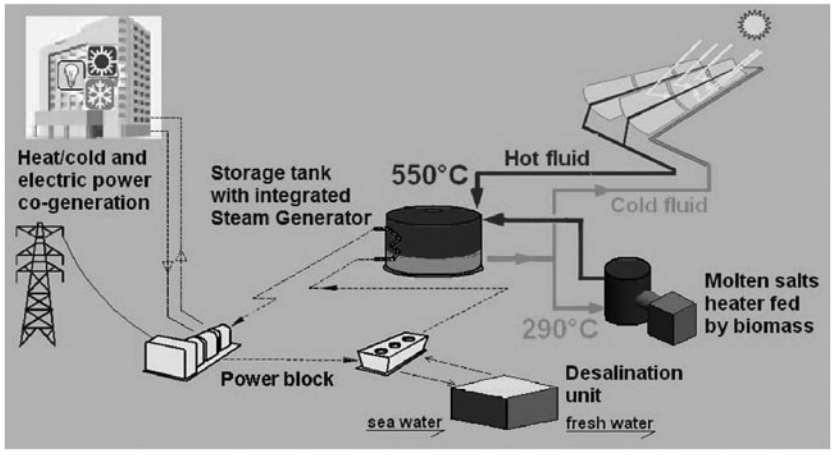

Fig. 1. Main components of MATS project.

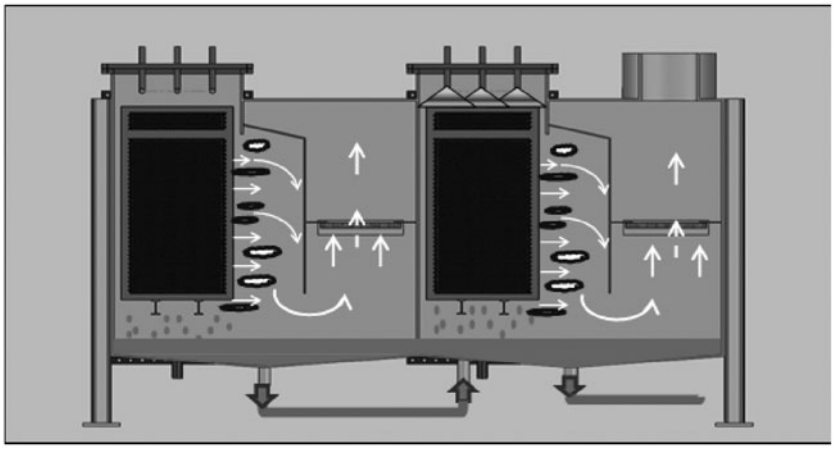

Fig. 2. Schematic diagram of MATS's MED-EC unit.

and droplet motion, in comparison with the experimental work of Phillips and Deakin [18]. They adopted the Eulerian–Lagrangian approach to calculate the trajectory of the liquid droplets coupling with the motion of the continued flow (flue gas), using flow data from Ansys CFX (commercial code). Standard k–ε and low Re k–ε turbulence models were used to solve the momentum equation of the continuous flow. Recently, Zhao et al. [19] conducted a numerical simulation of a waveplate demister with various geometries and operating conditions in order to study the separation efficiency, using FLUENT 6.1. They used the Lagrange approach in order to track the liquid droplets. The results showed that not only the vane spacing and flue gas velocity but also the vane height (including height of curve and upright region) and vane turning angles have a greater influence on the separation efficiency. There is no literature work on the CFD modeling of the MED wire mesh demisters except what was done by Rahimi and Abbaspour [20], and Al-Fulaij [21]. Rahimi and Abbaspour [20] predicated pressure drop in a mist pad using numerical simulation via CFD. They validated their numerical results with those obtained from the available experimental data and empirical models of El-Dessouky et al. [9]. With regard to the calculation of the separation efficiency, a detailed model for tracking the liquid droplets through the vapor field was not given. It is not clear in their work how the demister and flow of vapor and brine droplets were modeled. The separation efficiency was calculated on the basis of introducing certain amount of liquid water with the vapor flow and calculating the accumulated water at the bottom of the chamber.

Recently, Al-Fulaij [21] presented a numerical simulation model using the CFD procedure. The demister simulation was represented by two different methods: porous media and tube bank. The porous media approach follows the Eulerian–Eulerian modeling method, while two different models (Eulerian–Lagrangian and. Eulerian–Eulerian) were adopted to simulate the demister by the tube bank approach. In the Eulerian–Eulerian (multiphase) model, in the porous media or tube bank approach, a constant sink value was set for the porous media and for the fluid region around the tubes, in order to prevent brine droplet accumulation in the demister through simulations. However, the tube bank–discrete phase model approach followed the Eulerian–Lagrangian modeling method; in this model, the droplet particles escaped once they impacted the demister surface in order to be eliminated from the calculation. Most recently, Khamis and Fath [22] studied the influence of design of flash chamber configuration on thermal and hydraulic performances of the desalination unit, represented by calculations of demister separation efficiency and static pressure drop.

As far as the authors are aware, there is no published work on the effect of the separation baffles on the separation efficiency. The main purpose of this research is, therefore, to study the hydrodynamics behavior of vapor development inside MATS's MED-EC, and find feasibility of enhancing the separation performance (in terms of lowering the pressure drop and improving the carryover factor) through studying different designs of MED evaporator configurations.

2. Mathematical modeling

The simulation of the generated saturated vapor with the entrained water droplets was carried out through solving the governing equations for turbulent flow of continuous fluid "saturated vapor" coupled with solving the governing equations of the discrete fluid "water droplets." Physical properties of the continuous and dispersed fluid were taken as independent of temperature. Standard k–ε model was adopted as a turbulent model owing to its robustness and low computational time compared with the other turbulence models. On the other hand, the Eulerian–Lagrangian approach was implemented to trace the water droplets' motion and deposition. Assuming that the presence of droplets does not affect the continuous fluid flow (low concentration of droplets), the simulation of vapor droplets' flow through the demister consists of the calculation of a single-phase turbulent flow and the subsequent calculation of droplet motion.

2.1. Model assumptions

The following assumptions adopted in this study are: (i) steady-state, (ii) two-dimensional flow, (iii) demister as porous jump, (iv) incompressible Newtonian flow, (v) turbulent flow for vapor phase using k–ε model, (vi) isothermal flow so no heat/mass interaction between the gas phase and particles "inert exchange," (vii) the diameter of the liquid droplets is varied along the inlet width according to the Rosin–Rammler diameter distribution relationship, (viii) the liquid droplets have uniform shape as a sphere and they are stable during their movements, (ix) the forces acting on the particles are the Stokes drag of the vapor phase, and (x) the droplets are considered to rebound when they crash into any wall, except the demister where they are captured.

The continuous equation, the Navier–Stokes equation, and the k–ε equation of continuous phase are described as:

2.2. Conservation of mass

$$\frac{\partial u}{\partial x}+\frac{\partial v}{\partial y}=0 \tag{1}$$

2.3. Conservation of momentum

It is derived from Newton's second law that states that the rate of change of momentum equals the sum of forces acting on the fluid.

$$u\frac{\partial u}{\partial x}+v\frac{\partial u}{\partial y}=-\frac{1}{\rho}\frac{\partial P}{\partial x}+\nu\left[\frac{\partial^2 u}{\partial y^2}+\frac{\partial^2 v}{\partial x^2}\right] \tag{2}$$

$$u\frac{\partial v}{\partial x}+v\frac{\partial v}{\partial y}=-\frac{1}{\rho}\frac{\partial P}{\partial y}+\nu\left[\frac{\partial^2 u}{\partial x^2}+\frac{\partial^2 v}{\partial y^2}\right] \tag{3}$$

2.4. Transport equations for the standard k–ε model

The turbulence kinetic energy, k, and its rate of dissipation, ε, were obtained from the following transport equations:

$$\frac{\partial}{\partial x_j}(\rho k u_j)=\frac{\partial}{\partial x_j}\left[\left(\mu+\frac{\mu_t}{\sigma_k}\right)\frac{\partial k}{\partial x_j}\right]+\mu\frac{\partial u_i}{\partial x_j}\left[\frac{\partial u_i}{\partial x_j}+\frac{\partial u_j}{\partial x_i}\right]-\rho\varepsilon \tag{4}$$

$$\frac{\partial}{\partial x_j}(\rho\varepsilon u_k) = \frac{\partial}{\partial x_k}\left[\left(\mu + \frac{\mu_t}{\sigma_\varepsilon}\right)\frac{\partial \varepsilon}{\partial x_k}\right] + \frac{c_1\varepsilon}{k}\mu\frac{\partial u_i}{\partial x_j}\left(\frac{\partial u_i}{\partial x_j} + \frac{\partial u_j}{\partial x_i}\right) - c_2\rho\frac{\varepsilon^2}{k} \quad (5)$$

where μ_t is the turbulent velocity and was calculated with $\mu_t = 0.09$, $c_1 = 1.44$, $c_2 = 1.92$, $\sigma_k = 1.0$, and $\sigma_\varepsilon = 1.3$

In the Eulerian–Lagrangian model, the continuum phase is the fluid phase and it was solved using the Navier–Stokes equations, while the dispersed phase was solved by tracking the droplets through the flow field. The dispersed phase exchanges momentum and energy with the fluid phase. In order to solve the equation of motion of the dispersed phase, it is assumed that:

(1) The droplets are assumed as spheres.
(2) There is no droplet–droplet interaction.
(3) No slip velocity occurs between the droplets and the vapor.
(4) The droplet–film interaction at the walls is negligible.
(5) No liquid droplets break and no droplets are re-entrained.
(6) The acting forces are the drag force and Saffman's lift force [23].

Therefore, the equation of motion is reduced to the following expression:

$$\frac{du_p}{dt} = F_D(u - u_p) + F_x \quad (6)$$

F_x is an additional force, which is Saffman's lift force in this study; F_D is the drag force per unit particle mass, and can be obtained from:

$$F_D = \frac{18\mu}{\rho_p {d_p}^2}\frac{C_D Re}{24} \quad (7)$$

where u is the vapor velocity, u_p the droplets' velocity, μ the molecular viscosity of the vapor phase, ρ the vapor density, ρ_p the density of the droplets, t the relaxation time, and d_p the droplets' diameter. Re is the relative Reynolds number, which is defined as follows:

$$Re = \frac{\rho d_p|u_p - u|}{\mu} \quad (8)$$

The drag coefficient, C_D, for smooth particles can be taken from

$$C_D = a_1 + \frac{a_2}{Re} + \frac{a_3}{Re^2} \quad (9)$$

where a_1, a_2, and a_3 are constants that apply over several ranges of Re given by [24].

2.5. Reference case—original design

The MED-EC of MATS's project was selected as the reference case study in this work. The process datasheet of the reference unit is displayed in the Appendix. The simulation dimension and configuration of this unit is shown in Fig. 4.

2.6. Demister as porous material

The wire mesh mist eliminator, in the most general sense, is a simple porous blanket of metal or plastic wire that retains liquid droplets entrained by the vapor. As the vapor passes through the mist eliminator, droplets impinge on the extensive surface of the wire, and are retained until they coalesce into large drops. When liquid drops reach sufficient size, they break away from the wire mesh and fall back against the rising vapor stream, El-Dessouky et al. [9]. The performance of wire mesh eliminators depends on many design variables, such as wire diameter, packing density, pad thickness, and material of construction. Table 1 shows the values of those physical parameters for the case study of this work.

In this study, the demister was treated as a porous medium that has a finite thickness over which the pressure change is defined as a combination of Darcy's law and an additional inertial loss term:

Table 1
Specifications of the reference case's demister

Height (m)	Wire diameter (mm)	Packing density (kg/m3)	Surface area (m2/m3)	Porosity (%)
0.15	0.27	186.9	345	98

$$\Delta P = -\left(\frac{\mu}{\alpha} v + C_2 \frac{1}{2} \rho v^2\right) \Delta m \tag{10}$$

where μ is the laminar fluid viscosity, α is the permeability of the medium, C_2 is the pressure jump coefficient, nu is the velocity normal to the porous face, and Δm is the thickness of the medium. Appropriate values for α and C_2 can be calculated using the techniques described as follows:

$$\alpha = \frac{D^2}{150} \frac{\varepsilon^3}{(1-\varepsilon)^2} \quad \text{and} \quad C_2 = \frac{3.5}{D} \frac{(1-\varepsilon)}{\varepsilon^3} \tag{11}$$

where D is the mean mesh hole diameter and ε is the void fraction (porosity), defined as the volume of voids divided by the volume of the packed bed region.

2.7. Mesh generation and boundary conditions

Fig. 5 shows the mesh generated for the calculations. The grid consisted of 146,029 cells with a maximum volume of $3.84e^{-5}$ m^3. The grids were generated by meshing all faces, using regular quadrilateral mesh elements, and meshing the volume.

Both solution-adaptive refinement and boundary-adaptive refinement were used in the calculation with the coarse grid in order to get a reasonable solution. Due to the paper limit space, only the result of the grid independence test for reference case (Design-I) is presented in this work. As the flow was wall-dominated, the mesh extended into the viscous sublayer, such that y^+~1–5 in the wall-bounded mesh points, so that enhanced wall functions could be used with the k–ε turbulent model. The Eulerian–Lagrangian (Discrete phase model) calculation method was employed to predict droplet transport and deposition. A second-order upwind scheme was applied for space discretization of the governing equations. PRESTO and SIMPLE algorithms were adopted for the pressure interpolation and the velocity–pressure coupling, respectively. The turbulent stresses in the vapor momentum equation were modeled with the standard k–ε model. The solution attained its convergence after several hundreds of iterations with residuals less than 10^{-4} for the continuity, turbulence parameters, and momentum equations.

The inlet condition of vapor flow is the velocity inlet. The entering velocity of liquid droplets is assumed to be equal to the inlet velocity of water vapor. The outlet condition is outflow as shown in Fig. 6. The particle size distribution of droplets is assumed to be in agreement with the Rosin–Rammler diameter distribution. The maximum droplet sizes were taken as 1, 2, 3, 4, and 5 mm while the minimum sizes were 1, 2, 3, 4, and 5 μm, corresponding to each maximum diameter, respectively, and the spread parameter is 3.77. About 3,080 droplets were injected and distributed along the EC inlet section for each droplet size. Also, uniform liquid droplets having mean diameters of 1, 2, 3, 4, and 5 mm, respectively, were also investigated in order to compare the present study with the previous researches.

2.8. Model validation

The comparison with other references and the expression of the carryover factor, as will be defined in the following section, is not found in the literature. Therefore, in this section, for the sake of comparing with other references to validate the numerical model, the definition of separation efficiency would be used here alone. Separation efficiency is a measure to the fraction of droplets in the vapor swept out by the wire mesh mist eliminator, and is given by [9]:

$$\eta_{sp} = \frac{M_{in} - M_{out}}{M_{in}} \times 100 \tag{12}$$

M_{in} and M_{out} are the mass of entrained water droplet by the vapor up and downstream the demister, respectively.

The numerical calculations for separation efficiency and demister wet pressure drop were compared with those calculated from El-Dessouky's et al. [9] empirical correlation. The comparison was studied by the injection of three different liquid droplet sizes of 1, 3, and 5 mm, respectively. The entering vapor velocity was also taken as a uniform distribution of the computational domain of a Plexiglas column in the experimental work of El-Dessouky et al. [9]. A comparison of modeled and experimentally measured dependence of separation efficiency to vapor velocity is presented in Fig. 7. The results show that the simulated results agree well with the published experiments. The estimated uncertainties in the experimental work of El-Dessouky et al. [9] were 4.6 and 3.2% from the true values for the pressure drop of the wet demister and separation efficiency, respectively. Fig. 8 shows that there is good agreement between the theoretical results and calculated results of the empirical correlation with maximum deviation, including the experimental uncertainty of less than 19.16%; however, most of the disagreement between both results is under 10%. It was noticed that the computational model underpredicts most of the calculated

separation efficiency as shown in Fig. 8. The reason is attributed to the assumptions which are adopted in the discrete phase model, which causes the calculated results of the separation efficiency to be less than the experimental ones. In the numerical model, the - interaction between the droplets themselves and the interaction between the droplets and the droplet–film at the walls were neglected.

3. Results and discussion

In this study, the terminology of separation efficiency of MED-EC will be replaced by calculation of the carryover factor, where, at the design of the MED chamber, the number of droplets bounced back to the brine basin is larger than those of the MSF plant. This is attributed to the nature of the MED evaporator configuration. Therefore, the usage of the expression "carryover factor" would be more convenient in this study rather than the use of separation efficiency. The definition of the carryover factor is the ratio between the numbers of escaped droplets to the total number of injected droplets to the chamber.

$$\text{Carryover factor} = \frac{N_{esc}}{(N_{tr} + N_{fall} + N_{esc})} \times 100 \quad (13)$$

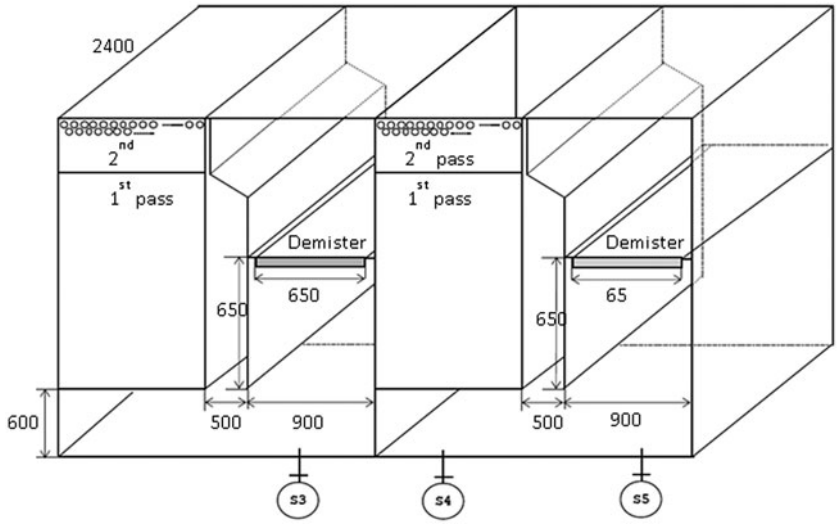

Fig. 3. Overall MED unit dimensions in mm.

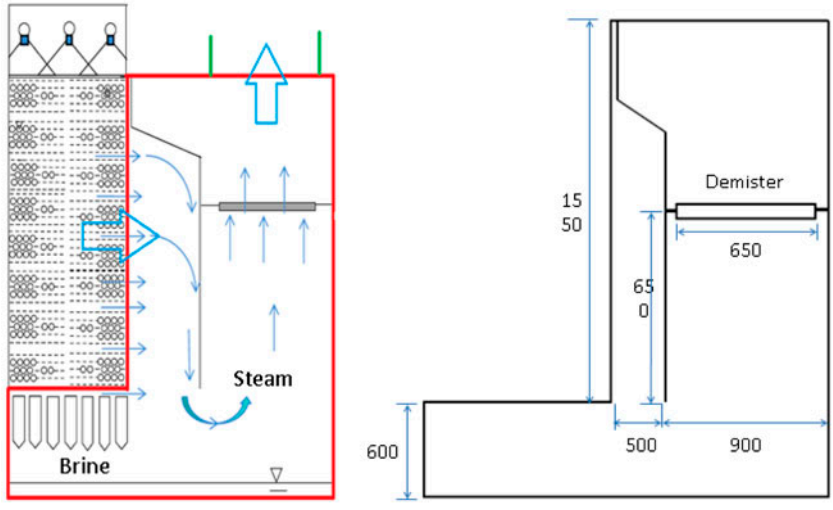

Fig. 4. Technical and process data of MATS's MED stage (dimensions in mm).

N_{tr} is the captured/trapped droplets' number by the demister, N_{esc} is the escaped droplets' number from the demister, and N_{fall} is the number of the droplets which fall down or bounce back to the brine i.e. does not complete its journey to the demister

The assessment of the MED evaporator chamber in terms of the carryover factor and pressure drop for the three different designs is conducted here in this section. The assessment is carried out through the effect of the variation of the entering vapor velocity on the chamber performance.

Three different separation baffle designs will be presented. Design-I stands for the reference design of MED evaporator (see Figs. 2 and 3), Design-II is a

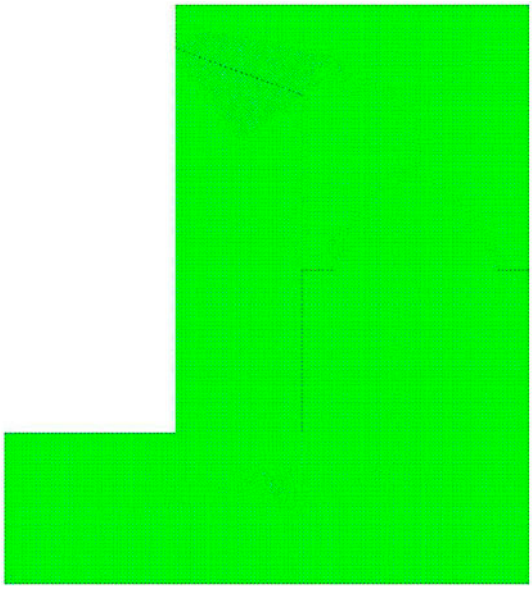

Fig. 5. Mesh grid generation.

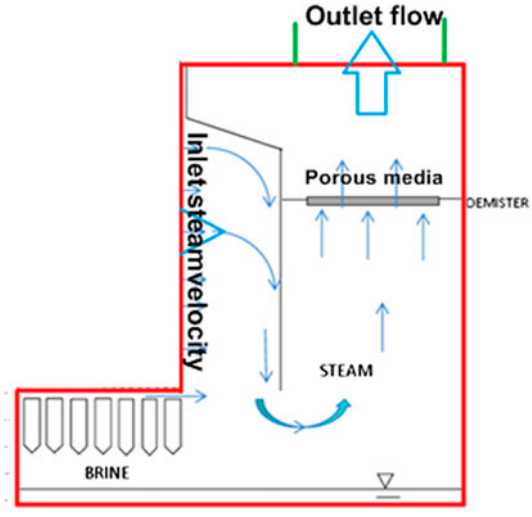

Fig. 6. Schematic diagram for boundary conditions.

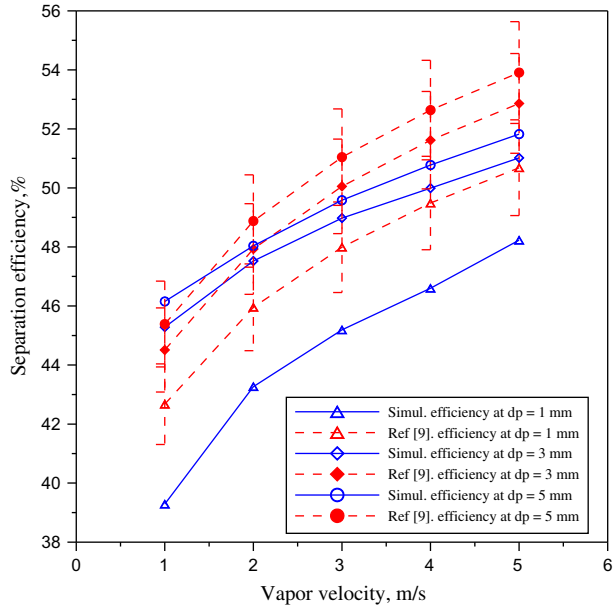

Fig. 7. Comparison of the published experimental and modeled separation efficiency at various vapor velocities.

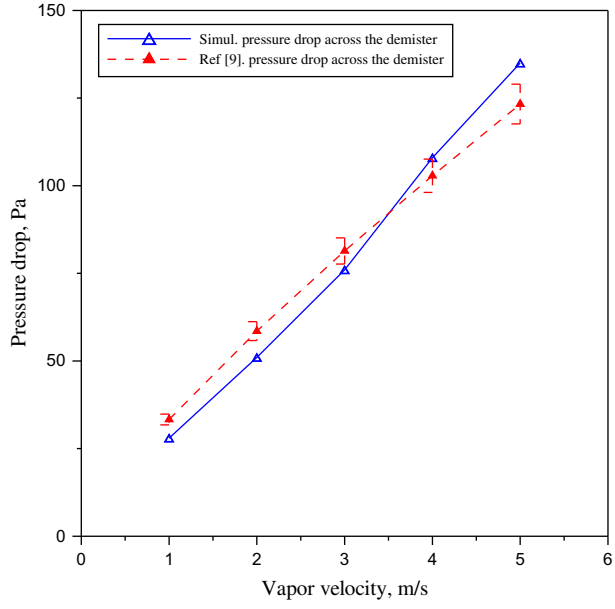

Fig. 8. Comparison of the published experimental and modeled demister pressure drop at various vapor velocities.

modification of the reference design by removing the vertical baffle plate at the vapor entrance, while Design-III is for a perforated baffle instead of solid one in the reference design.

3.1. Design-I: "the reference design"

The main objective of the vertical baffle is to divert the generated vapor path lines from its direction to the demister directly, thus enabling the droplets that have larger size to fall down at the bottom of the evaporator chamber. On the other hand, the droplets that have smaller diameters complete their journey to the demister. However, the change of momentum direction of the droplets that have smaller diameters causes part of those droplets to collide with the opposing wall to the baffle and then be redirected to the demister. Therefore, the demister is exposed to severe non-uniform entering velocity, and this encourages the lift force to control the number of escaping droplets through the demister. The change of vapor momentum at the baffle gains, however, the droplets' extra inertia, which enables the demister to capture them easily. The increase in the inlet vapor velocity augments the inertia impact with the demister, and accordingly, this enhances

Table 2
The effect of entering steam velocity on the separation efficiency for Design-I

V m/s	Escaped	Trapped	Incomplete	Carry-over factor	ΔP (Pa)
0.5	1,926	180	974	0.625	3
1	1,883	38	1,159	0.6114	5
1.5	1,886	4	1,190	0.6123	13
2	1,932	15	1,133	0.627	24
2.5	1,968	5	1,107	0.639	38
3	2,018	14	1,048	0.6552	54
3.3	2,062	12	1,006	0.669	67
3.5	2,078	15	987	0.6747	74
4	2,077	17	986	0.6743	95
4.5	2,086	20	974	0.677	121
5	2,086	21	973	0.677	148

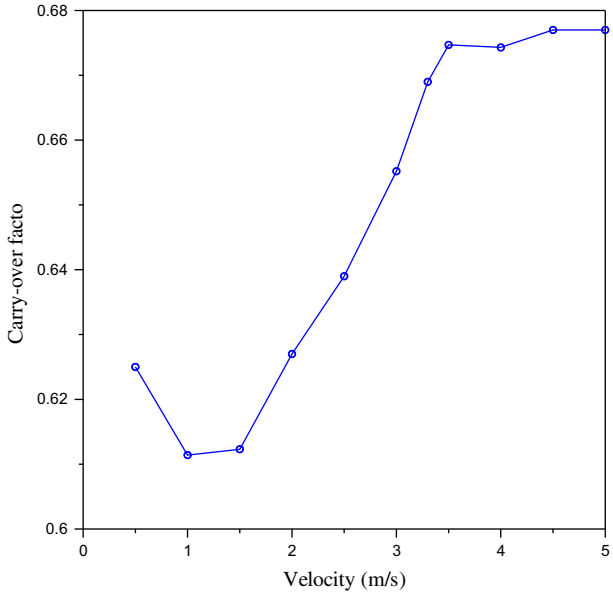

Fig. 9. The effect of inlet vapor velocity variations on the carryover factor for Design-I.

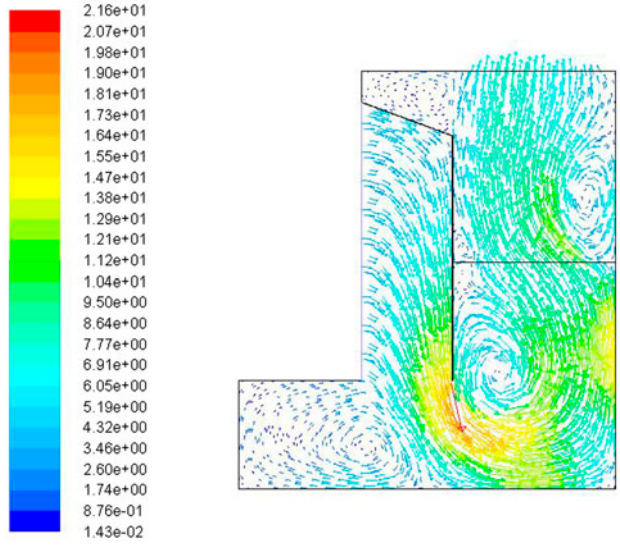

Fig. 10. The velocity contours of the reference design of the MED evaporator at inlet vapor velocity.

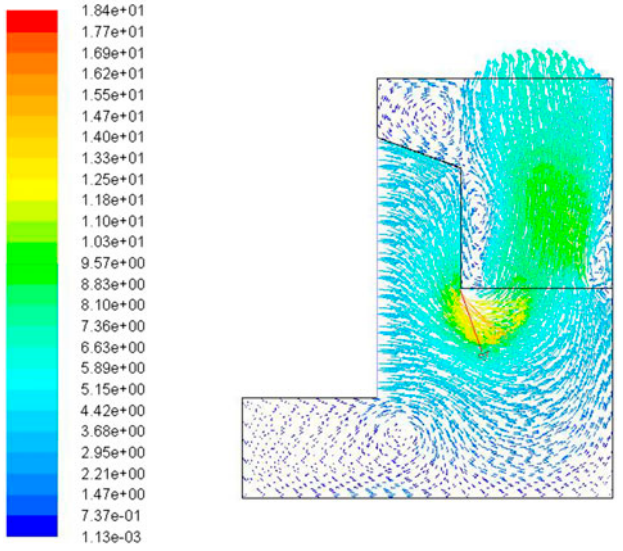

Fig. 11. The velocity contours of the second design of the MED evaporator at inlet vapor velocity.

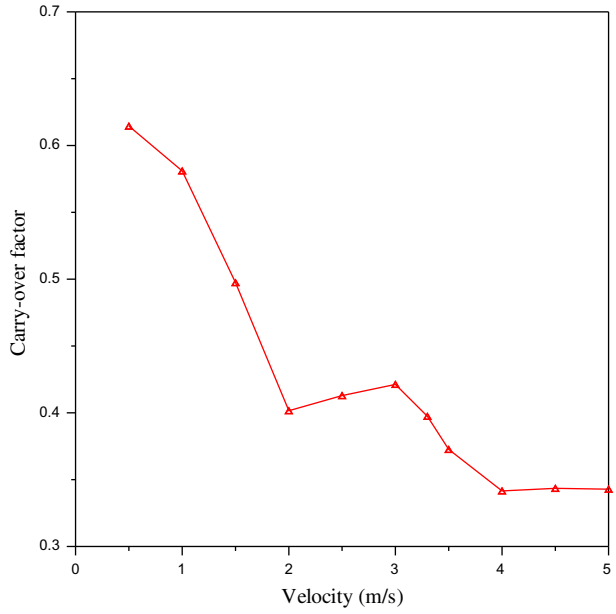

Fig. 12. The effect of inlet vapor velocity variations on the carryover factor for Design-II.

the performance of the demister. Alternatively, the increase in the inlet vapor velocity causes severe variation in the entering vapor velocity along the demister width, thus also augmenting the lift force, which worsens the performance of the demister. Therefore, the two competitive forces work simultaneously. The net outcome of this competition is recorded in Table 2 and Fig. 9.

Fig. 10 shows the vapor velocity contours distributed all over the evaporator chamber. The presence of the vertical baffle creates vortices around the baffle edge and causes impingement of flow pathlines with the opposing wall of the baffle and chamber demister. In Table 2, the increase in the entering vapor velocity accounts for an increase in the number of escaped droplets from the demister as a result of the augmentation of the lift force. On the other hand, the number of falling (incomplete) droplets increases with an increase of the entering vapor velocity until the velocity reaches 1.5 m/s; after this value, the increase of the vapor inlet velocity causes the falling droplets' number to decrease. The explanation of this is that at the beginning of increasing vapor velocity up to 1.5 m/s, the generated vortices are not strong enough to entrain those droplets to the demister, and accordingly, the droplets fall by their weight into the brine. After $v = 1.5$ m/s, the increase in the vapor velocity empowers those vortices to carry the droplets up and

Table 3
The effect of entering steam velocity on the carryover for Design-II

V m/s	Escaped	Trapped	Incomplete	Carryover factor	ΔP (Pa)
0.5	1,905	649	546	0.6145	2
1	1,801	540	759	0.581	5
1.5	1,542	522	1,036	0.4974	11
2	1,245	607	1,248	0.4016	19
2.5	1,280	517	1,303	0.4129	30
3	1,306	452	1,342	0.4213	42
3.3	1,232	502	1,366	0.3974	52
3.5	1,155	538	1,407	0.3726	58
4	1,059	581	1,460	0.3416	75
4.5	1,065	610	1,425	0.3435	95
5	1,063	672	1,365	0.3429	118

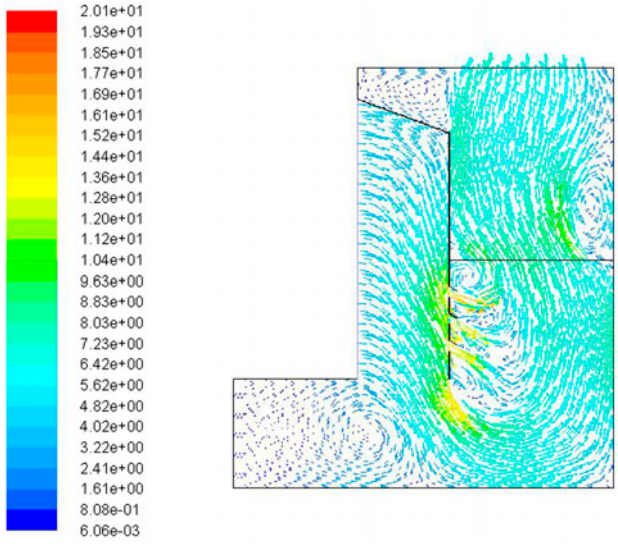

Fig. 13. The velocity contours of the third design of the MED evaporator at inlet vapor velocity.

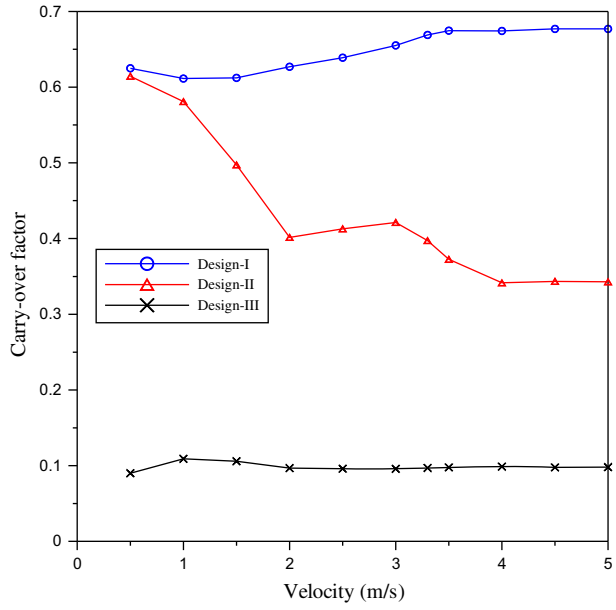

Fig. 14. Comparison between the three different designs in terms of the chamber carryover factor.

overcome their body forces, and thus reduces the number of falling droplets. The net product of the influence of velocity variations on the chamber carryover factor is depicted in Fig. 9. As shown in this figure, at low velocities of 1–1.5 m/s, the evaporator chamber is featured by a low carryover factor. This indicates that the lower velocity favors the performance of the demister to efficiently capture the droplets; the lower velocity also permits a large portion of the droplets to fall down into the brine by its gravity. Furthermore, the collision with the vertical baffle or demister at a lower velocity is weak; this wanes the lift force to carry the smallest droplets up to the demister. Therefore, it can be summarized that the present design of the MED evaporator should operate at a lower velocity, below 1.5 m/s, to have a lower carryover factor and reasonable pressure drop at the demister.

3.2. *Design-II: "without the presence of the vertical baffle"*

Similar results were obtained for Design-II where the baffle section below the demister is removed. Fig. 11 shows the velocity contours of Design-II of the MED evaporator, and Table 3 illustrates the effect of entering vapor velocity on the carryover factor.

Again, the contrast effects of lift and inertia forces cause erratic behavior for the evaporator chamber of Design-II. As shown in Fig. 12, the increase in vapor inlet velocity up to 2 m/s enhances

Table 4
The effect of entering steam velocity on the carryover for Design-III

V m/s	Escaped	Trapped	Incomplete	Carryover factor	*P* (Pa)
0.5	276	554	2,250	0.09	2
1	336	369	2,375	0.109	5
1.5	326	284	2,470	0.1058	12
2	298	142	2,640	0.0967	21
2.5	296	67	2,717	0.096	33
3	295	78	2,707	0.0958	48
3.3	299	66	2,715	0.097	58
3.5	301	62	2,717	0.0977	65
4	304	41	2,735	0.0987	85
4.5	301	20	2,759	0.0977	106
5	302	17	2,761	0.098	132

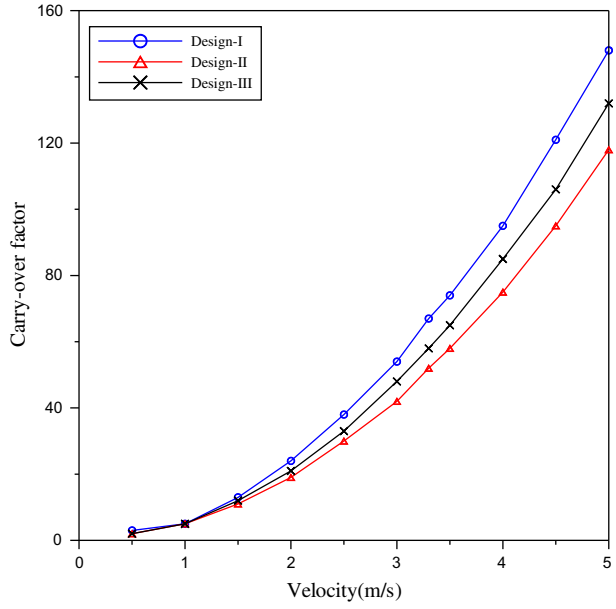

Fig. 15. Comparison between the three different designs in terms of the demister pressure drop.

the evaporator performance by reducing the carryover factor. Then, the carryover trend goes up until $v = 3$ m/s, and then declines again until $v = 4$ m/s, and it is almost a fixed constant after this value. The main benefit of removing the vertical baffle is the reduction of the vortices' number compared with those in Design-I, thus reducing the demister pressure drop and the number of entrained small droplets to the demister.

3.3. Design-III: "with a perforated vertical baffle"

Fig. 13 shows the velocity contours of the third design of the MED evaporator at the inlet vapor velocity, while Table 4 illustrates the effect of entering vapor velocity on the carryover for Design-III

As noticed from Fig. 13, the third design is characterized by almost uniform velocity along the demister width, and the number of vortices is reduced as a result of the presence of inclined openings inside the vertical baffle. These openings (or holes) damp the turbulence intensity of the vapor flow around the baffle, and consequently, it is expected that the carryover factor of the evaporator chamber is enhanced as in Fig. 14. Table 4 is prepared to emphasize this perception by listing the number of escaping, trapped, and incomplete droplets. As observed from this table, the number of escaped droplets in this design is considered to be smaller than those in case of Design-I and Design-II. In addition, the new design of the separation baffles enables the evaporator to retrieve most of the entrained droplets with the flowing vapor to the demister, and then reduces the salinity of the fresh product from the unit.

With regard to the comparison of the three different designs in terms of the demister pressure drop in each EC configuration, Fig. 15 presents this comparison. As seen in this figure, Design-III, which characterizes the lowest carryover factor, has an intermediate pressure drop among the three different designs. This is a consequence of the mitigation of the turbulence vortices produced by the new proposed design "Design-III".

4. Conclusion

CFD numerical study for the vapor flow inside the MED - EC has been presented with a proposed new design for the separation baffle configuration. The trajectory of liquid droplets has been calculated using the Eulerian–Lagrangian method. The continuity and Navier–Stokes equations for the continuous phase "vapor" have been solved simultaneously with the particle equation. Different designs of MED separation baffle configurations have been studied and three are presented for the effect of separation baffle configuration on the baffle–demister thermal and hydraulic performances. In this study, the thermal performance is represented by the demister pressure drop, which is translated to a drop in the vapor saturation temperature. The hydraulic efficiency is represented by the carryover factor. The following major conclusions can be drawn:

(1) Design-I (reference design of the separation baffle) has the highest demister pressure drop associated with the highest carryover as a result of the high generation of vortices around the vertical baffle.
(2) Design-II (with removal of the separation baffle below the demister) is attributed by the lowest demister pressure drop with relative reduction in its carryover factor compared with that of Design-I.
(3) Design-III (with perforated vertical baffle) has the best performance in terms of the lowest carryover factor among all designs with a reasonable pressure drop for the demister.

The study could be considered a benchmark and helpful guideline in the design of future evaporator configuration in MED desalination plants.

Acknowledgments

Computing infrastructure for this research was provided by grants from the European–Egyptian MATS (Multipurpose Applications by Thermodynamics Solar) and the European Union Seventh Framework Programme (FP7/2007-2013), Grant Agreement Number 268219. The authors would like to acknowledge this support.

Nomenclature

d — diameter, m
EC — evaporation Chamber
F_x — additional acceleration (force/unit particle mass) term in x direction, m/s^2
g_x — gravitational acceleration in x direction, m/s^2
M — mass flow rate, kg/s
m — demister thickness, m
N — number of water droplets
P — pressure, Pa
k — rate of kinetic energy
Re — reynolds number
u — velocity in x direction, m/s
v — velocity in y direction, m/s
x — position x, m
y — position y, m
t — time, s

Greek letters

ρ — density, kg/m^3
μ — dynamic viscosity, Pa.s
α — permeability of the medium, m
ε — rate of kinetic energy dissipation
Δ — difference
η — efficiency

Subscripts

i — coordinate in i direction
in — inlet
out — outlet
esc — escaped
tr — trapped
$fall$ — fall down
j — coordinate in j direction
p — particle
m — mixture
tm — turbulent stress mixture
sp — separation efficiency

References

[1] A. Ophir, F. Lokiec, Advanced MED process for most economical sea water desalination, Desalination 182 (2005) 187–198.
[2] M. Al-Shammiri, M. Safar, Multi-effect distillation plants: State of the art, Desalination 126 (1999) 45–59.
[3] K.C. Ng, K. Thu, M.W. Shahzad, W. Chun, Progress of adsorption cycle and its hybrids with conventional multi-effect desalination processes, IDA J. Desalin. Water Reuse 6(1) (2014) 44–56.
[4] K. Thu, Y-D. Kim, G. Amy, W.G. Chun, K.C. Ng, A hybrid multi-effect distillation and adsorption cycle, Appl. Energy 104 (2013) 810–821.
[5] M. Wakil Shahzada, K.C. Ng, K. Thu, B. Baran Saha, W. Gee Chun, Multi effect desalination and adsorption desalination (MEDAD): A hybrid desalination method, Appl. Thermal Eng. (2014), in press. Available from: http://www.sciencedirect.com/science/article/pii/S1359431114002439.
[6] D.-C. Alarcón-Padilla, L. García-Rodríguez, Application of absorption heat pumps to multi-effect distillation: A case study of solar desalination, Desalination 212 (2007) 294–302.
[7] D.C. Alarcón-Padilla, L. García-Rodríguez, J. Blanco-Gálvez, Experimental assessment of connection of an absorption heat pump to a multi-effect distillation unit, Desalination 250 (2010) 500–505.
[8] D.-C. Alarcón-Padilla, L. García-Rodríguez, J. Blanco-Gálvez, Design recommendations for a multi-effect distillation plant connected to a double-effect absorption heat pump: A solar desalination case study, Desalination 262 (2010) 11–14.
[9] H. El-Dessouky, I. Alvtiiq, H. Ettouney, N. Al-Deffeeri, Performance of wire mesh mist eliminator, Chem. Eng. Process. 39 (2000) 129–139.
[10] E. Brunazzi, A. Paglianti, Design of wire mesh mist eliminators, Am. Inst. Chem. Eng. J. 44 (1998) 505–512.
[11] I. Langmuir, K.B. Blodgett, US Army Air Forces Technical Report 5418, 1946.
[12] J. Pich, Aerospace Science, C.N. Davies (Ed.), Academic Press, New York, NY, 1966 (Chapter 9).
[13] C.L. Carpenter, D.F. Othmer, Entrainment removal by a wire mesh separator, Am. Inst. Chem. Eng. J. 1 (1955) 549–557.
[14] E. Brunazzi, A. Paglianti, Design of complex wire mesh-mist eliminators, Am. Inst. Chem. Eng. J. 4 (2000) 1131–1137.
[15] Y. Wang, G.A. Davies, CFD studies of separation of mists from gases using vane-type separators, Chem. Eng. Res. Des. 74 (1996) 232–238.
[16] I. Gillandt, C. Riehle, U. Fritsching, Gas-particle flow in a comparison of measurements and simulations, Forschung Im Ingenieurwesen—Eng. Res. 62 (1996) 315–321.
[17] Y. Wang, P.W. James, The Calculation of wave-plate Demister efficiencies using numerical simulation of the flow field and droplet motion, Chem. Eng. Res. Des. 76 (1998) 980–985.
[18] H. Phillips, A.W. Deakin, Measurements of the collection efficiency of various demister devices, Proceedings of the Fourth Annual Meeting of the Aerosol Society, Loughborough, 1990.
[19] J. Zhao, B. Jin, Z. Zhong, Study of the separation efficiency of a demister vane with response surface methodology, J. Hazard. Mat. 147 (2007) 363–369.
[20] R. Rahimi, D. Abbaspour, Determination of pressure drop in wire mesh mist eliminator by CFD, Chem. Eng. Process. 47 (2008) 1504–1508.
[21] H.F.Al-Fulaij, Dynamic Modeling of Multi Stage Flash (MSF) Desalination Plant, PhD-thesis, London, (2011).

[22] M. Khamis Mansour, H.E.S. Fath, Numerical simulation of flashing process in MSF flash chamber, Desalin. Water Treat. 51 (2013) 2231–2243.
[23] P.G. Saffman, The lift on a small sphere in a slow shear flow, J. Fluid Mech. 22 (1965) 385–400.
[24] H.P. Chen, Computational Fluid Dynamics, Water Conservancy and Hydroelectricity Publications, Beijing, 1995, pp. 97–103.